Coarsening through directed droplet coalescence in fluid-fluid phase separation

Snigdha Thakur,[1] Pramod A. Pullarkat,[2] and P. B. Sunil Kumar[1]
[1]*Department of Physics, Indian Institute of Technology Madras, Chennai 600036, India*
[2]*Raman Research Institute, Bangalore 560080, India*
(Received 1 April 2009; published 31 July 2009)

Phase-separation dynamics of an asymmetric mixture of an isotropic dopant in a nematogenic fluid is presented. We show that, on steady cooling, the nucleating nematic drops move down the dopant concentration gradient, with a velocity that is dependent on the cooling rate and concentration gradient. This propulsion of the drops leads to a mechanism of droplet coarsening, where radius of a drop scales with time as $R(t) \sim t$. Various mechanisms for droplet propulsion are discussed.

DOI: 10.1103/PhysRevE.80.011708 PACS number(s): 83.80.Xz, 64.70.M−, 64.75.Cd

I. INTRODUCTION

Phase separation is a commonly observed phenomenon in various systems including metals, simple liquids, and complex fluids such as polymers and liquid crystals [1]. The dynamics of phase separation in nematic liquid crystals has received considerable attention for the past many years, both experimentally [2–5] and theoretically [6,7].

Mixtures containing nematogenic and nonmesogenic (isotropic) components have attracted considerable interest both technologically and scientifically [8]. For example, polymer-dispered liquid crystals, which are produced using phase separation of polymers and liquid crystals, are widely applied in electro-optic devices [9]. Recently theoretical investigations were carried out on the phase ordering kinetics in such mixtures [10]. Here, one has two competing dynamics: one dominated by the transition from isotropic to nematic ordering of the liquid crystal and another determined by the phase separation of the isotropic component from the liquid crystal, where anisotropy affects solubility. In isotropic fluid-fluid phase separation, for asymmetric mixtures, the coarsening is mainly characterized by two mechanisms, with the early stage growth of domains described by the "evaporation-condensation" mechanism, where the domain size $R(t) \sim t^{1/3}$ and the late stage mechanism involving droplet diffusion and coalescence again characterized by $R(t) \sim t^{1/3}$ [11]; here $R(t)$ is the radius of the drops at time t.

Recently, we have shown [12] that adding nonmesogenic impurities to the liquid crystal makes the phase-separation dynamics surprisingly rich. We have provided a very clear experimental demonstration of a mechanism for coarsening through self-propelled motion of nematic drops nucleating from the mixture. We also proposed a mechanism for the self-propulsion of drops as that induced by the surface flow resulting from the asymmetric concentration of an expelled impurity. Such mechanisms may be important in material processing as, for example, in the preparation of polymer dispersed liquid crystals [13] and other composite materials. Here we provide a detailed study of our proposed mechanism of self-propulsion induced by the phase separation of ordered-disordered liquid mixture and its effects on the coarsening dynamics. We show that the growth rate of drops is given by $R(t) \sim t$, both on steady cooling and following a quench.

The paper is organized as follows. In Sec. II we briefly describe the experimental procedures and explain our results. Section III elaborates the possible mechanism of drop propulsion. In Sec. IV, we describe the model for phase separation in detail. The results from the numerical simulation of the model are listed in Sec. V. We conclude the paper with a summary in Sec. VI.

II. EXPERIMENTS

We carried out experiments using mixtures of a common liquid crystalline compound and some isotropic dopants (details of the components are given below). In an earlier paper we had reported some of the experimental observations on phase separation in these mixtures, where we concentrated mainly on the propulsion of drops [12]. We saw that, when a uniform mixture is cooled across its *I-N* transition temperature, nematic droplets nucleate throughout the sample cell. These nematic drops exhibited a remarkable coalescence dynamics. Small droplets drifted toward bigger domains and coalesced with it, resulting in a few fast growing domains. A Marangoni flow, resulting from the concentration-dependent isotropic-nematic interfacial tension, was shown to be the reason for the directed motion of the droplets. In Fig. 1 we show the asymmetric concentration profile of the nonmesogenic compound around the drops leading to a difference in surface tension across the drop. In this paper we look at the growth rate of the drops and investigate its propulsion mechanism in more detail.

Experiments were performed on an asymmetric mixture of 4-octyloxy-4′-cyano-6-biphenyl with 10–20 wt % of an isotropic dopant. Two different dopants were used for measurements: (i) fluorescent perlyene labeled polystyrene oligomers and (ii) hardner of the commercially available two-component epoxy Araldite. Mixtures were filled in a glass cell with dimensions 1 cm × 1 cm × 18 μm in the isotropic state. The temperature during the experiments was controlled by a homemade hot stage with an accuracy of 0.1 °C. Fluorescence microscopy and polarized light microscopy were carried out using a Zeiss Axiovert 135 microscope and a high gain electron multiplying charge coupled device camera. We consider two cases: (a) a steady cooling and (b) a temperature quench. In the case of steady cooling we look at the cases of (i) starting from a uniform back ground and (ii) starting from a pre-exisitng gradient in the concentration.

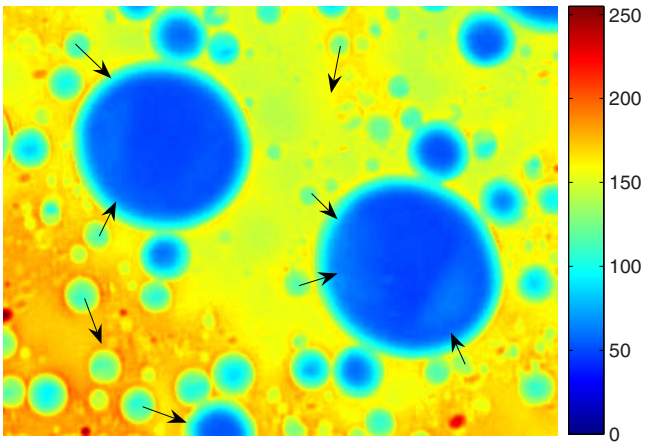

FIG. 1. (Color online) Pseudocolor fluorescence (impurity is fluorescent) image of nematic drops formed in a sample starting from uniform concentration. The dopant concentration is asymmetric in the case of small moving drops. The arrows indicate the direction of motion for a few drops.

A. Steady cooling from a pre-existing gradient

When a sample with radially decreasing concentration of nematogen, in its isotropic phase, is cooled at a steady rate, we see the drops nucleating progressively away from the center and moving toward the center of the region. Such a radial concentration profile can be obtained by the following procedure. A sample with uniform concentration in the isotropic phase is cooled such that a big nematic domain is formed. Upon heating this nematic domain melts and the expelled impurity starts to diffuse in radially. This fast cycling through the *N-I-N* transitions results in a radial profile of the relative concentration in the sample (see Ref. [12] for details). The drift velocity of the drop, in the presence of a radial concentration gradient, is shown in Fig. 2, as a function of time. The velocity and growth of the drops depend on the cooling rates. For a fixed cooling rate, the drop velocity remains almost constant while it grows at a constant rate. The drift velocity itself is an increasing function of the cooling rates.

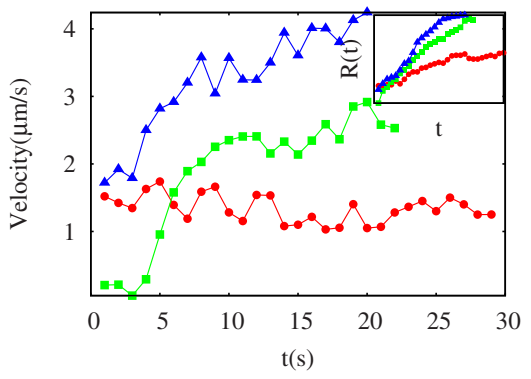

FIG. 2. (Color online) A typical velocity plot of a drop in the presence of radial gradient in the relative concentration, for cooling rates 0.2 (filled ○), 0.5 (filled □), and 1.0 °C/min (filled △). Inset shows the radius of these drops as a function of time for the same time interval. High cooling rate implies higher growth rate. $t=0$ is the time at which the drop becomes visible.

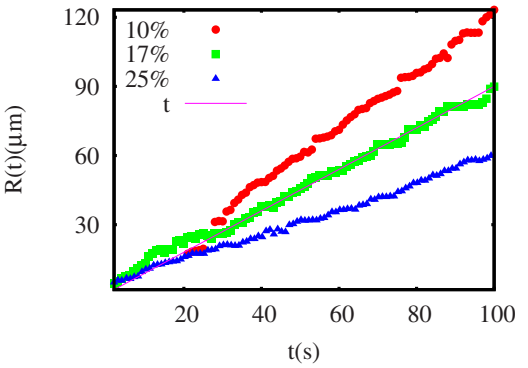

FIG. 3. (Color online) Averaged radius of drops as a function of time at a fixed cooling rate of 1.0 °C/min; the curves from top to bottom are for impurity concentrations of 10 (filled ○), 17 (filled □), and 25 wt % (filled △). The continuous line indicate growth law $R(t) \sim t$.

B. Steady cooling from a uniformly mixed sample

Figure 3 shows the radii of the moving drops as a function of time, when cooled from a uniform mixture at a fixed cooling rate, for different impurity concentration. The radius of the drops scales as $R(t) \sim t$. As expected, when the impurity concentration is increased growth rate of the drops decreases. We observe a linear increase in the drop size at all stages of the growth. Surprisingly, we do not see any dependence of the overall impurity concentration on the velocity of the drop, indicating that only asymmetry in the concentration around the drop matters. Figure 4 shows the velocity of the drops at a cooling of 1.0 °C/min for three different impurity concentrations.

C. Temperature quench from a uniformly mixed sample

Coarsening of the drops was also studied following a temperature quench. Phase separation in these experiments was triggered by transferring a uniformly mixed sample without any pre-existing gradient to an unstable two-phase region. In experiments this was achieved by transferring the sample from one hot stage to another hot stage, which provides us an extremely high quench rate. The expelled impurity, from the

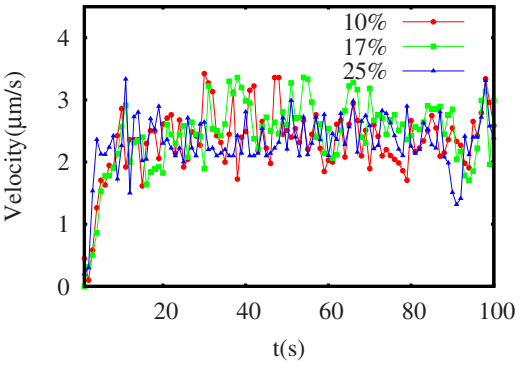

FIG. 4. (Color online) Velocity of the drops as a function of time at a fixed cooling rate of 1.0 °C/min for impurity concentrations of 10 (filled ○), 17 (filled □) and 5 wt % (filled △).

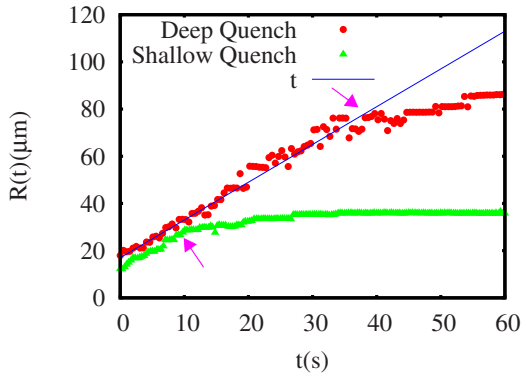

FIG. 5. (Color online) Averaged radius of the domains as a function of time, under different degree of quench for a sample with 17 wt % impurity. Filled ○ (top) is when the sample is quenched from 95 to 64 °C. Filled △ (bottom) is when the sample is quenched from 95 to 68 °C. Arrows indicate the time when domains stopped moving. The continuous line indicate growth law $R(t) \sim t$.

first few nematic domains that are nucleated, sets up a gradient in the concentration around it. The domains that are nucleated subsequently drift along this gradient and coalesce with the big domains. We thus see a few static big domains and many small domains that move toward it. Once the impurity concentration outside the nematic domains increases nucleation and directed drift of the drops stop. Further growth of the domains is only through the diffusive coalescence of the drop. When the domain growth is primarily through the directed motion of drops, the radius $R(t)$ increased linearly with time. While diffusive coalescence gives rise to a growth law $R(t) \sim t^{1/3}$ [14]. We show in Fig. 5 average radius of the domains as a function of time. As expected we clearly see two regimes with the above growth laws. For shallow quench (95–68 °C) the duration of linear growth is smaller than the deep quench (95–64 °C). The isotropic-nematic transition temperature of the above sample is 70 °C.

III. POSSIBLE MECHANISM OF PROPULSION

There are a number of possible mechanisms leading to propulsion of drops [15–21]. Our experimental conditions and results rule out some of them as unsuitable. We discuss them in detail here. Motion due to convective currents can be ruled out as there is no hydrodynamic flow field away from the moving drop, which we verify by observing a freely suspended micron-sized particles. The fact that the drop motion stops when cooling stops rules out any possibility of dipolar interactions as a possible mechanism. We also rule out any forces coming from the nematic anchoring at the surface as glass plates treated for different specific alignments do not affect the motion. Since the drop motion is observable for many cycles of cooling and heating in the same sample, chemical reactions cannot be the reason for such motion of drops.

One possible mechanism for the drop motion, which is applicable here, is that proposed by Karpov and Oxtoby [19].

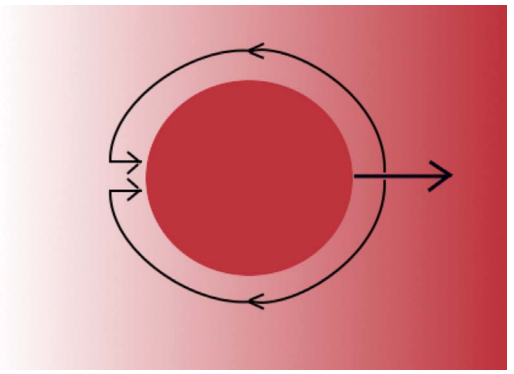

FIG. 6. (Color online) Schematic of the surface flow and drop propulsion.

Presence of background concentration gradient and the expulsion of impurity from nucleating nematic droplets gives rise to an asymmetric concentration profile around the drop (shown in Fig. 1). This results in an asymmetric interfacial tension, which sets up a surface flow around the drop and propels the drop forward. Schematic diagram of the surface flow and drop propulsion is shown in Fig. 6. In the next section we will describe a model coupling the isotropic-nematic phase transition to the phase-separation process.

IV. MODEL

The essential feature of the experiments described above is that the nonmesogenic impurity is expelled by the nematic domains. The concentration gradient of this impurity is the driving force for the drop motion. Though the liquid crystal-isotropic transition is used here to demonstrate the self-propulsion phenomenon, it should be observable in any other systems wherein the dynamics of a conserved order parameter is coupled to a nonconserved order parameter. The model incorporates two different mechanisms for propulsion of drops: one driven by a concentration dependent surface tension and another a chemical-potential-driven flow around the drop. The model is similar in spirit to that proposed in Ref. [10]. The phase-separation dynamics is described by the coupled dynamics of two order parameters, a conserved field ϕ, which describes the relative concentration, and nonconserved field S, which describes the phase of the system. For the experiments given here $\phi = \frac{\rho_n - \rho_i}{\rho_n + \rho_i}$, with ρ_n as the nematogen concentration and ρ_i as the concentration of isotropic component. $\phi > 0$ corresponds to nematogen-rich phase, the orientational order $S=0$ in the isotropic phase, and $S>0$ in the nematic phase.

To describe the isotropic-nematic transition, we employ the following free-energy functional for the orientational order [22]:

$$\mathcal{F}_{IN} = \frac{1}{2}a(\phi)S^2 - \frac{1}{3}wS^3 + \frac{1}{4}uS^4, \tag{1}$$

where

$$a(\phi) = a_0[\phi^* - \tanh(a_1\phi)].$$

$a(\phi)$ models the concentration dependence of the nematic-isotropic transition temperature in mixtures. a_0 is a linear function of temperature, and $\phi^*(T)$ sets the critical concentration for the isotropic-nematic transition at a temperature T. $a(\phi)$ also provide the coupling between the concentration field and the nematic order parameter.

Mixing and demixing of the phases are described by the Landau free energy,

$$\mathcal{F}_{mix} = \frac{1}{2}b\phi^2 + \frac{1}{2}[(1+\phi)\log(1+\phi) + (1-\phi)\log(1-\phi)], \tag{2}$$

where second term is the entropy of mixing. We have set $k_BT=1$ and $b>0$. Thus, the total free-energy functional of the system is given as

$$\mathcal{F} = \mathcal{F}_{IN} + \mathcal{F}_{mix} + \frac{1}{2}(\sigma_0 + \sigma_1\phi)(\nabla S)^2. \tag{3}$$

Here σ_0 and σ_1 determine the concentration dependence of the interfacial tension. $a_0(T)$, a_1, w, u, and b are phenomenological coefficients. The equations of motion for ϕ and S are then given by

$$\Gamma_S^{-1}\frac{\partial S}{\partial t} = -\frac{\delta\mathcal{F}}{\delta S} + \eta_s, \tag{4}$$

and

$$\Gamma_\phi^{-1}\frac{\partial \phi}{\partial t} = \nabla^2\frac{\delta\mathcal{F}}{\delta\phi} - \mathbf{V}\cdot(\nabla\phi) + \eta_\phi, \tag{5}$$

where,

$$\frac{\delta\mathcal{F}}{\delta S} = a(\phi)S - wS^2 + uS^3 - (\sigma_0+\sigma_1\phi)\nabla^2 S,$$

$$\frac{\delta\mathcal{F}}{\delta\phi} = -\frac{a_0a_1S^2}{2}\mathrm{sech}^2(a_1\phi) + b\phi + \frac{\sigma_1}{2}(\nabla S)^2.$$

η_s and η_ϕ determine the strength of thermal noise in Eqs. (4) and (5). For simplicity we neglect the effect of fluctuations and set η_ϕ and η_s to zero. The advection of the order parameter by the velocity field $\mathbf{V}$ has been taken into account by the term $\nabla\cdot(\mathbf{V}\phi)$, which appears in Eq. (5), using the incompressibility condition for the fluid $\nabla\cdot\mathbf{V}=\mathbf{0}$, as $\mathbf{V}\cdot(\nabla\phi)$. From Eqs. (4) and (5) it is clear that while $a(\phi)$ models the effect of impurity on the nematic-isotropic transition, it also provides a linear term in ϕ in Eq. (5) making the nematic order parameter act as a local field [11]. It is thus the nematic field that drives the phase separation here.

The velocity field $\mathbf{V}$ is coupled to the concentration field through the force $\phi\nabla\mu$. Here μ is the chemical potential given by $\mu=-\partial\mathcal{F}/\partial\phi$. The Navier-Stokes equation for the velocity field of the fluid is then

$$\rho\left(\frac{\partial\mathbf{V}}{\partial t} + (\mathbf{V}\cdot\nabla)\mathbf{V}\right) = \mathbf{F}_\phi - \nabla\mathbf{P} + \eta\nabla^2\mathbf{V} \tag{6}$$

where, $\mathbf{F}_\phi=\phi\nabla\mu$, P is the pressure, and η is the viscosity of the fluid. The term F_ϕ in Eq. (6), arising from the chemical-potential gradient, acts as a driving force for the transport of the fluid. $\phi\nabla\mu$ is the force arising from the free-energy change per unit volume that accompanies the transport of a fluid region with order parameter ϕ over a distance for which the change in the chemical potential is $\nabla\mu$ [11]. In the overdamped limit (appropriate to most experimental systems), for small velocities, the left-hand side of above equation can be set to zero. The resulting linear equation for $\mathbf{v}$ can be solved in Fourier space,

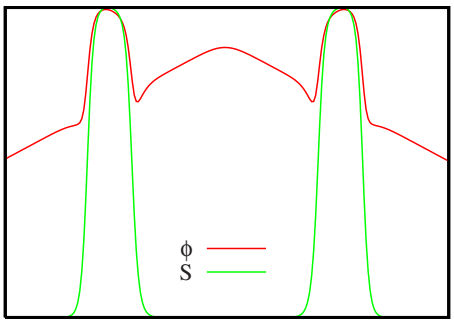

FIG. 7. (Color online) The variation in the nematic order parameter S and the concentration order parameter ϕ along a line through the center of the drops in a tentlike gradient. Drops were nucleated on either sides of the tentlike gradient.

$$v_\alpha(k) = \frac{1}{\eta k^2}(-ik_\alpha p(k) + F_{\phi_\alpha}(k)). \tag{7}$$

Assuming the fluid to be incompressible we can eliminate the pressure and obtain, in the Fourier space, the velocity components to be,

$$v_{k_\alpha} = \frac{F_\beta}{\eta k^2}\left(\delta_{\alpha_\beta} - \frac{k_\beta k_\alpha}{k_\alpha k_\alpha}\right) \tag{8}$$

We numerically solve Eqs. (4) and (5) by using an explicit Euler scheme by discretizing space and time. We use the correlation length for concentration fluctuation $\zeta=\sqrt{b}$ as the unit of length and Γ_S^{-1} as the unit of time. For numerical stability we choose $\Delta x=\zeta/2=1$ and $\Delta t=0.005\Gamma_S^{-1}$. We set $a_1=3$, $w=20$, and $u=w-a_0[\phi^*-\tanh(a_1)]$ such that the minima of the nematic free energy are at $S=0,1$ and $\phi=1$. We look at the effect that different values of a_0 and ϕ^* have. We use a box of size L with periodic boundary in all directions and set $\Gamma_\phi^{-1}/\Gamma_S^{-1}=10$.

V. NUMERICAL RESULTS

In our experiments [12] we saw nucleating drops expelling impurity and moving up the nematic concentration gradient. These experiments indicated that the presence of background gradient may be the driving mechanism for propulsion of drops (see Fig. 6). In order to verify this, using our model proposed above, we simulated the motion of drops nucleated at either sides of a linear tentlike gradient. The calculations show that, in the presence of such a background gradient, the nucleating drops expel impurity out of it and move down the impurity gradient (or up the gradient of nematogen). The motion of the drops in a background concentra-

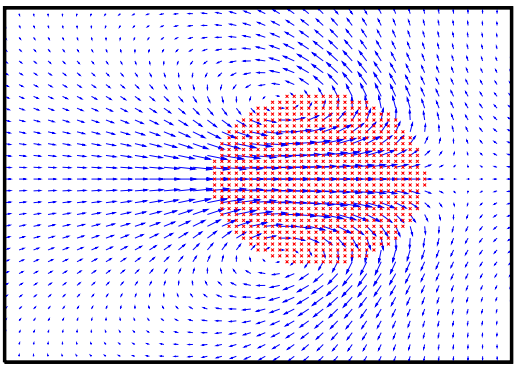

FIG. 8. (Color online) The velocity field in and around the moving drop [shaded (red) region] when $\sigma_0=10$ and $\sigma_1=5$. Drop is moving in a tentlike gradient toward the right. Only a small part of the full system is shown for clarity.

tion with a hill at the center is shown in supporting movie 1 [24]. Figure 7 shows the variation in the nematic order parameter S and the concentration order parameter ϕ in and outside the drops (only a line through the center of the drops is shown for clarity). Figure 8 shows the flow field around the drop. We clearly see two vortices and the resulting surface flow propelling the drop in the direction of positive nematic gradient. Such a flow could result from the concentration dependent surface tension (modeled by the σ_1 term) or from the flow resulting from the difference in ∇S at the leading and trailing edges of the drop originating from the first term in Eq. (1). We also confirmed that the drop motion is not seen when there is no gradient in the system. Below we look at the effect of the concentration dependent surface tension in more detail.

A. Effect of σ_1 in the drop propulsion

In the model presented above, the interfacial tension has concentration-independent (σ_0) and concentration-dependent (σ_1) terms [see Eq. (3)]. As mentioned earlier drop motion was observed even in the absence of σ_1. The velocity profile obtained in this case, which is quite different from the one that originates with σ_1 term, is shown in Fig. 9. Making

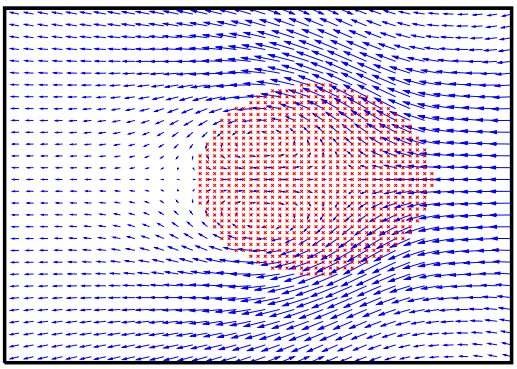

FIG. 9. (Color online) The velocity field in and around the moving drop [shaded (red) region] when $\sigma_0=10$ and $\sigma_1=0$. Drop is moving in a tentlike gradient toward the right. Only a small part of the full system is shown for clarity.

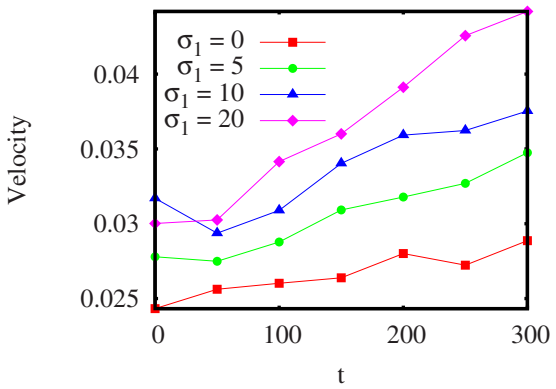

FIG. 10. (Color online) Velocity of the moving drop as a function of time for different values of σ_1, with $\sigma_0=10$, $a_0=18$, and $\phi^*=0.9$, for a fixed tentlike gradient in the x direction with $\phi=0.7$ at $x=0.0$ and $\phi=0.3$ at $x=\pm L/2$. Time t is scaled in units of Γ_S^{-1} and length in $\zeta/2$.

$\sigma_1 \neq 0$ increases velocity of the drops significantly. The surface flow resulting from this term can be seen in Fig. 8.

Figures 10 and 11 show the velocity and growth of the moving drop for different σ_1 values, with $\sigma_0=10$. σ_1 not only affects the movement of the drop but also plays a crucial role in determining the growth rate of the drop. This is shown in Fig. 11. Higher σ_1 implies larger gradient and mean value of the surface tension. The former will lead to larger value of the drop velocity, while the latter limits its growth rate. We also see that the radius of the drop scales as $R(t) \sim t$, which is in accordance with our experimental observation (see Fig. 3).

B. Effect of cooling

In the experiments we observed an increase in drift velocity upon increasing the cooling rate. In the model the effect of changing temperature can be included by changing the values of a_0 and/or ϕ^*. To obtain a comparison with experiments we looked at the effect of changing a_0 and ϕ^* in a system with a radial gradient in concentration such that ϕ is maximum at the center. For a given value of a_0 there is a

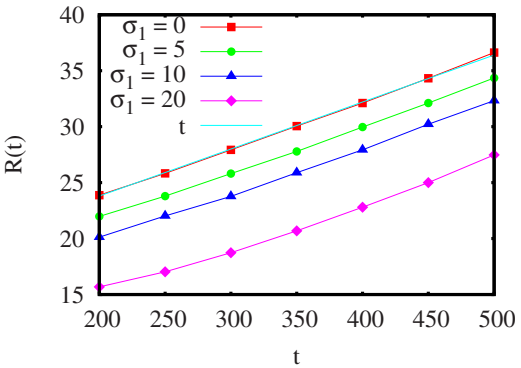

FIG. 11. (Color online) Radius of a domain as a function of time as it moves up a tentlike gradient in the x direction with $\phi=0.7$ at $x=0.0$ and $\phi=0.3$ at $x=\pm L/2$ for different σ_1 keeping $\sigma_0=10$, $a_0=18$, and $\phi^*=0.9$. Time t is scaled in units of Γ_S^{-1} and length in $\zeta/2$.

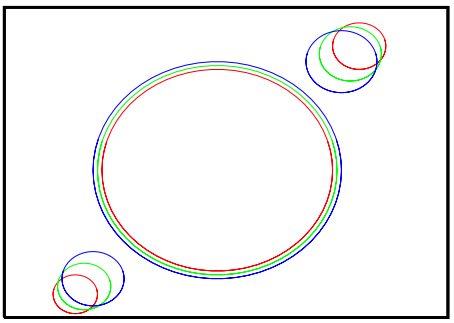

FIG. 12. (Color online) The radial drift and growth of droplets are illustrated by stacking the detected boundaries of domains at different times. Domain boundaries are approximated as circles for clarity. Similar radial drift was observed in our earlier work (see Fig. (1b) in [12]).

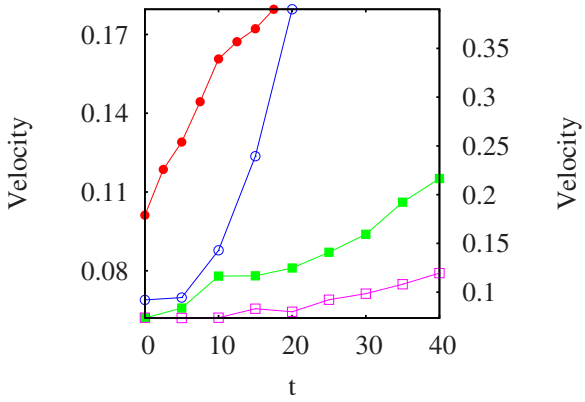

FIG. 13. (Color online) Velocity of the drop as a function of time for two different rates of decrease of ϕ^* and a_0. Filled symbols are when $a_0=18$ with ϕ^* decreasing (left axis), from 0.9, at the rate of 10^{-5}/step (filled ○) and 10^{-6}/step (filled □). Open symbols are for the cases where $phi^*=0.9$ and a_0 is decreased, from 18 (right axis), at the rate of 10^{-3}/step (open ○) and 10^{-4}/step (open □). The results are for a fixed radial gradient with $\phi=0.7$ at the center and $\phi=0.3$ at the boundary. Time t is scaled in units of Γ_S^{-1} and length in $\zeta/2$.

critical ϕ^* above which the domains do not grow for any $\phi<1$. As we decrease ϕ^* the minimum ϕ that allow for domain growth decreases. Thus change in ϕ^* is akin to changing the temperature of the sample. Similar effect can be obtained by changing a_0 for a given value of ϕ^*.

In the simulations we first nucleate a drop at the center; the ϕ^* and a_0 are chosen such that this drop grows up to a certain size. Since we have a radial gradient in ϕ, for a given ϕ^* and a_0, domain can nucleate and grow only up to a certain distance from the center. As we decrease ϕ^* or a_0 drops can nucleate and grow farther away from this central domain. These drops feel the ϕ gradient and move toward the big domain at the center as shown in Fig. 12 and in supporting movie 2 [24]. Figure 13 shows the velocity of a drop in the radial gradient for two different rates at which ϕ^* and a_0 are decreased. It is very clear that the drop moves much slowly when the rates are low similar to the effect of cooling rates seen in experiments.

We also find that when two drops are close by, a short-range attractive force seems to pull them toward each other. We observe that an overlap in the local concentration fields is responsible for this attractive interaction. Such a mechanism, induced by capillary instability, has been proposed by Tanaka [23].

VI. SUMMARY

The experimental observations and numerical calculations from the model, presented here, clearly support a surface-flow-induced propulsion of nematic domains. We consider two different mechanisms that can give rise to such flows and show that a concentration-dependent surface tension can greatly enhance the velocity of the domains. We could rule out the effects of forces induced by a concentration-dependent anchoring energy at the substrates [21]. However such a differential anchoring energy at the nematic-isotropic interface could also give rise to a concentration-dependent surface tension, which is not explicitly modeled here. In conclusion, we have proposed a model for phase-separation in a mixture of an ordered fluid and a disordered fluid. We show that in the presence of a background concentration gradient, nucleating drops exhibit self-propulsion. The observed domain coarsening follows $R(t)\sim t$, which is different from that seen in coarsening due to diffusive coalescence or evaporation-condensation mechanisms, where $R(t)\sim t^{1/3}$. This phenomenon may be important in the preparation of polymer dispersed liquid crystals wherein concentration gradients driven by phase separation and coarsening could add an additional level of complexity.

ACKNOWLEDGMENTS

We thank N. V. Madhusudana for discussions. S.T. acknowledges DAAD, Germany and CSIR, India for support. We thank the referee for pointing out the PDLC applications.

[1] A. Onuki, *Phase Transition Dynamics* (Cambridge University Press, Cambridge, 2002).
[2] I. Chuang, N. Turok, and B. Yurke, Phys. Rev. Lett. **66**, 2472 (1991).
[3] A. N. Pargellis, S. Green, and B. Yurke, Phys. Rev. E **49**, 4250 (1994).
[4] P. Ziherl and S. Žumer, Eur. Phys. J. E **12**, 361 (2003).
[5] F. Mercuri, U. Zammit, F. Scudieri, and M. Marinelli, Phys. Rev. E **68**, 041708 (2003).
[6] H. Tanaka and T. Araki, Phys. Rev. Lett. **81**, 389 (1998).
[7] C. Denniston, E. Orlandini, and J. M. Yeomans, Phys. Rev. E **64**, 021701 (2001).
[8] J. I. Fukuda, Phys. Rev. E **59**, 3275 (1999).
[9] J. W. Doane, N. A. Vaz, B.-G. Wu, and S. Žumer, Appl. Phys.

Lett. **48**, 269 (1986).
[10] T. Araki and H. Tanaka, Phys. Rev. Lett. **93**, 015702 (2004).
[11] A. J. Bray, Adv. Phys. **43**, 357 (1994).
[12] S. Thakur, P. B. Sunil Kumar, N. V. Madhusudana, and P. A. Pullarkat, Phys. Rev. Lett. **97**, 115701 (2006).
[13] J. B. Nephew, T. C. Nihei, and S. A. Carter, Phys. Rev. Lett. **80**, 3276 (1998).
[14] I. Lifshitz and V. Slyozov, J. Phys. Chem. Solids **19**, 35 (1961).
[15] R. Golestanian, T. B. Liverpool, and A. Ajdari, Phys. Rev. Lett. **94**, 220801 (2005).
[16] Y. Sumino, N. Magome, T. Hamada, and K. Yoshikawa, Phys. Rev. Lett. **94**, 068301 (2005).
[17] J. Nardi, R. Bruinsma, and E. Sackmann, Phys. Rev. Lett. **82**, 5168 (1999).
[18] *Modelling and Simulation of Capsules and Biological Cells*, edited by C. Pozrikidisi (Chapmann & Hall/CRC, New York, 2003).
[19] V. G. Karpov and D. W. Oxtoby, Phys. Rev. E **55**, 7253 (1997).
[20] N. Vladimirova, A. Malagoli, and R. Mauri, Phys. Rev. E **60**, 2037 (1999).
[21] A. D. Rey, Liq. Cryst. **26**, 913 (1999).
[22] J. Prost and P. de Gennes, *The Physics of Liquid Crystals* (Claredon Press, Oxford, 1995).
[23] H. Tanaka, J. Chem. Phys. **105**, 10099 (1996).
[24] See EPAPS Document No. E-PLEEE8-80-175907 for movies, from numerical simulations on the motion of the drops, with a background concentration profile having (1) one dimensional linear gradient with a maximum at the center and (2) a radial concentration gradient. For more information on EPAPS, see http://www.aip.org/pubservs/epaps.html.